Journal of Materials Research and Technology 29 (2024) 3355–3365

Contents lists available at ScienceDirect

Journal of Materials Research and Technology

journal homepage: www.elsevier.com/locate/jmrt

Role of micro- and nano-cobalt ferrite as an additive in enhancing the viscous behaviour of magnetorheological grease

S.M.A. Tarmizi [a], N.A. Nordin [a,*], S.A. Mazlan [a,b], S.A.A. Aziz [c], U. Ubaidillah [d,e,**], M.A.F. Johari [a], M.H.A. Khairi [a]

[a] Engineering Materials and Structures (eMast) iKohza, Malaysia-Japan International Institute of Technology (MJIIT), Universiti Teknologi Malaysia, Jalan Sultan Yahya Petra, 54100, Kuala Lumpur, Malaysia
[b] Department of Mechanical Engineering, College of Engineering, University of Business & Technology (UBT), P.O. Box No 21448, Jeddah, Saudi Arabia
[c] Faculty of Applied Sciences, Universiti Teknologi MARA (UiTM), Cawangan Pahang, Kampus Jengka, 26400 Bandar Tun Abdul Razak, Pahang, Malaysia
[d] Department of Mechanical Engineering, Faculty of Engineering, Universitas Sebelas Maret, Surakarta, 57126, Indonesia
[e] Mechanical Engineering Department, Islamic University of Madinah, Madinah Al Munawwarah, 42351, Saudi Arabia

ARTICLE INFO

Handling editor. P.Y. Chen

Keywords:
Additives
Cobalt-ferrite
Magnetic grease
Microparticles
Nanoparticles
Viscous behavior
Fibrous structure

ABSTRACT

The incorporation of micro- and nanosized additives offers a significant potential solution to improve the viscous behavior which can minimize energy consumption and surpass pumpability demonstrated by magnetorheological grease (MRG). The role of the additives utilized, on the other hand, has piqued the interest of researchers. Therefore, cobalt-ferrite ($CoFe_2O_4$) in micro- (M) and nanosized (N) as an additive incorporated in this study to reduce the initial off-state viscosity and simultaneously maintain the resultant shear and yield stress of MRG during on-state conditions. To analyze the viscous behavior effect of MRG types, the samples underwent rheological tests in different parameters. Then, MRG was dried to elucidate the morphological changes. The results showed that micro-sized additives recorded the lowest off-state viscosity with 43.2 % of reduction, followed by nano-$CoFe_2O_4$ (26 %) and pure grease. It is due to M has shortened and disentangled the fibrous structures of grease thickener whilst N has filled in the voids among the thickener which contributed to the discharged of base oil thus reduced the viscosity of MRGs. Meanwhile, at on-state conditions, M1 and N1 exhibited enhanced performances of yield and shear stress as compared to pure MRG, O attributed to the improved magnetic attraction among particles in the grease medium. These findings are beneficial for MRG to be employed in MR devices for various purposes.

1. Introduction

Magnetorheological (MR) grease, which is composite grease embedded with magnetic particles, particularly carbonyl iron particles (CIP) has piqued the interest of many scholars due to its promising and tremendous properties over the last decade [1–7]. The semi-solid state and thixotropic properties exhibited by the grease has significantly encountered the sedimentation and leakage issues that occurred in fluid-type MR materials [8,9]. When an external magnetic field is induced to this magnetic composite, the magnetic dipoles of magnetic particles would tend to align along with the direction of magnetic fields resulting in the formation of particles' chain-liked structure in the grease. The change in the structure has improved the viscous behavior of the MRG including shear stress and yield stress, which then denoted to the stability and strength of the material [10,11]. Therefore, MR grease has the potential to be used in advance devices, particularly semi-active brakes [12–14], clutches [15,16] and dampers [17,18]. Commonly, high-speed devices require MR grease with high viscosity during the operation (on-state condition) to generate high yield stress and, maintain its chain-like structure under high stress with presence of magnetic fields. However, in the absence of applied magnetic field, which corresponds to the off-state condition of MR grease, a high viscosity that exhibited by the fibrous structure of grease has drawbacks, especially during the initial-state of operation which indirectly causes pumpability suffers and necessitates more power consumption for the devices to begin operating [14,19]. Therefore, finding a solution to reduce the

* Corresponding author.
** Corresponding author. Department of Mechanical Engineering, Faculty of Engineering, Universitas Sebelas Maret, Surakarta, 57126, Indonesia
E-mail addresses: maisarahtarmizi94@gmail.com (S.M.A. Tarmizi), nurazmah.nordin@utm.my (N.A. Nordin), ubaidillah_ft@staff.uns.ac.id (U. Ubaidillah).

https://doi.org/10.1016/j.jmrt.2024.01.219
Received 10 November 2023; Received in revised form 21 January 2024; Accepted 24 January 2024
Available online 2 February 2024

off-state viscosity of MRG, while maintaining its high yield stress during the operation is needed. A liquid-type of additive has been introduced by many researchers to overcome the issue of high off-state viscosity of MR grease including kerosene [13,20,21], silicone oil [22] and castor oil [20]. These liquid additives work as a lubricant in the medium, where the oil would fill-up the spaces between thickening agents and breaks up the three-dimensional (3D) structure of grease [23]. Even though by adding liquid additive can lower the initial viscosity of grease, however, the yield stress of MR grease has also been affected due to the slipping effect that occurs between the particles under the shear stress [13]. Alternatively, solid additives have been introduced to achieve the improvement target.

As for now, a few types of solid additives have been successfully utilized and improved the viscous behavior of MR grease including chromium oxide (CrO_2) [24], molybdenum disulphide (MoS_2) [25], graphite (Gr) [26] and cobalt ferrite ($CoFe_2O_4$) [19,27]. A study [24] showed that introducing nano-CrO_2 into the MRG has significantly improved the stability and enhanced the yield stress of the material up to 95 % as the magnetic field was applied, in which the additive has been worked as a stabilizer in the grease medium. This study however mainly focused to enhance the yield stress of the material at the on-state condition. Meanwhile, Mohamad et al. [28] has utilized the nanoparticles which was maghemite, γ-Fe_2O_3 that resulted a remarkable effect on the reduction the off-state viscosity of MRG to ~800 Pa s as compared to ~10000 Pa s in MRG without γ-Fe_2O_3. In fact, when the magnetic field was applied, the presence of nanoparticles during the alignment of magnetic particles has filled-up the empty spaces between the micro-size of CIP, resulting in the increased of the viscosity of MRG. Nevertheless, the extent to which the effect of yield stress of MRG with γ-Fe_2O_3, particularly at the on-state condition was still undebated. In fact, the used of γ-Fe_2O_3 as additive in the MRG might not result in the maximum effect as the additive has primarily possessed antiferromagnetic behavior which would deteriorate the resultant magnetic responsiveness of MRG towards the applied magnetic field [29,30].

Despite the fact that the nano-sized additives have been successfully enhanced the properties of MRG, however, in liquid-medium like MRF, few studies [31–35] stated that the presence of bigger size of solid additives, particularly up to micro-size particles have promoted better effects toward the viscosity enhancement and simultaneously improved the sedimentation stability of the material. For instance, Molazemi et al. [32] employed different sizes of $CoFe_2O_4$ particles from 60 nm to 0.55 μm in the MRF and discovered that the strength of the material has been increased with larger size of the $CoFe_2O_4$. In fact, the larger size of additives could improve the shear stress of MRF up to 20 %, particularly at the on-state condition due to greater magnetic interactions and cross-linking network generated among the particles [33,35]. On the other hand, a research [19] has been carried out by introducing the micro-sized of $CoFe_2O_4$ particles in order to reduce the off-state viscosity of MRG. The result showed that the off-state viscosity has been reduced by 86 % as compared to the MRG without $CoFe_2O_4$. In fact, the study also emphasized the improvement in shear stress and yield stress of MRG with the micro-particles of $CoFe_2O_4$, about 36 % increment. All these studies somehow provide ambiguous information on which sizes; either micro- or nanoparticles additives could proffer more effectiveness towards the property's modification of MRG, particularly on the off-state viscosity reduction and on-state yield stress enhancement.

The studies of additives thus far have been discovered to influence the rheological performance of MRG however, the knowledge about the role of the additive sizes in altering the structural of MRG that predominantly contribute to the change in corresponding properties is considerably limited. Therefore, the aim of this present work is to investigate the significant changes in viscous behavior of MRG as well as the shear and yield stress that contained two different sizes of solid additive. For this purpose, $CoFe_2O_4$ has been chosen due to promising advantages such as strong anisotropy, good chemical stability and high mechanical strength [36–39] that is expected to provide most effective approach towards the desired properties of MRG composite. The synthesized $CoFe_2O_4$ has been sintered at different temperatures to obtain respective different sizes of micro- and nano-particles. Then, MRG samples were prepared with 1 wt % of micro- and nanoparticles of $CoFe_2O_4$ separately, and the findings has been compared with the pure MRG without $CoFe_2O_4$ and also the previous works. All prepared samples were examined in terms of rheological properties respective to viscosity, shear stress and yield stress, and the correlation between different sizes of $CoFe_2O_4$ particles towards the rheological and structural changes in MRG further intensified.

2. Materials and methodology

2.1. Synthesize and characterizations of $CoFe_2O_4$ particles

The co-precipitation method [27,40–42] was used to synthesize the $CoFe_2O_4$ particles. In this method, 1.0 mol of iron nitrate ($Fe(NO_3)_3 \bullet 9H_2O$ and 0.5 mol of cobalt acetate ($Co(CH_3COO \bullet 4H_2O$) that were purchased from Merck, Spain were mixed with 1.0 mol of distilled water. Then, the mixture was stirred with a magnetic stirrer hot plate at 100 °C for 2 h. Afterward, a few drops of sodium hydroxide, NaOH that acted as an extracting agent were added into the mixture until black precipitates were obtained. The mixture was then left in the room temperature until the formation of bilayers between the precipitated at bottom and wastewater on top was observed. Next, the liquid was poured out and the precipitated was washed few times until the desired pH of 13 was achieved since high alkalinity would result in high magnetic saturation [43,44]. After the desired pH was obtained, the precipitates were then be filtered and washed with acetone to remove impurities. The precipitates were dried in a furnace at 200 °C for 24 h in order to remove the moisture contained [45]. As a result, a form of black powder, $CoFe_2O_4$ was collected. The $CoFe_2O_4$ was then grounded with mortar and pestle to gain finer powder. The fined powder was further divided into two portions that underwent sintering process at the temperature of 1000 °C and 500 °C, respectively for 8 h, to obtain different sizes of micro- and nano-particles of $CoFe_2O_4$. Then, the micro-particles of $CoFe_2O_4$ were denoted as M, while the nanoparticles were denoted as N. The process is summarized in Fig. 1.

In order to determine the morphology of the synthesized $CoFe_2O_4$ particles, field emission scanning electron microscope (FESEM, Hitachi SU8020, Japan) with 5 kV of power supply were used. On the other hand, the elemental composition of particles was analyzed by using an X-Ray diffraction, XRD (Empyream, Pan Analytical) with the set scan of Cu K_α, where k is the source radiation at 0.154 nm. The scan was done within the Brag's angle range of 20° to 80°. Meanwhile, the magnetic properties of the particles were examined in terms of the magnetization (M_s), coercivity (H_c) and retentivity (M_r) via vibrating sample magnetometer, VSM from Lakeshore 7404 Series, USA. The applied magnetic fields were ranging from −14k to 14 kA/m and the test was done at room temperature.

2.2. Fabrication and characterizations of MRG

Prior to the fabrication of MRG composite, 30 wt % of grease was stirred for 5 min to loosen the internal structure of the based grease using a mechanical stirrer at 300 rpm. Afterward, 70 wt % of carbonyl iron particles, CIP was added into the stirred grease and the mixture was continuously stirred for 2 h to ensure the homogenous distribution of CIPs in the grease [8,46]. The mixture was denoted as MRG and was labeled as O. Meanwhile, for the MRG with 1 wt % of $CoFe_2O_4$ as an additive, particularly for each micro- and nano-sized particles, 29 wt % of grease would be used while the 70 wt % of CIP was maintained. The mixture was then stirred continuously for 2 h at 300 rpm. The samples were denoted as M1 and N1 which indicated the MRG with 1 wt % of micro-sized $CoFe_2O_4$ and MRG with 1 wt % of nano-sized $CoFe_2O_4$, respectively. The summary of all samples including the fabricated

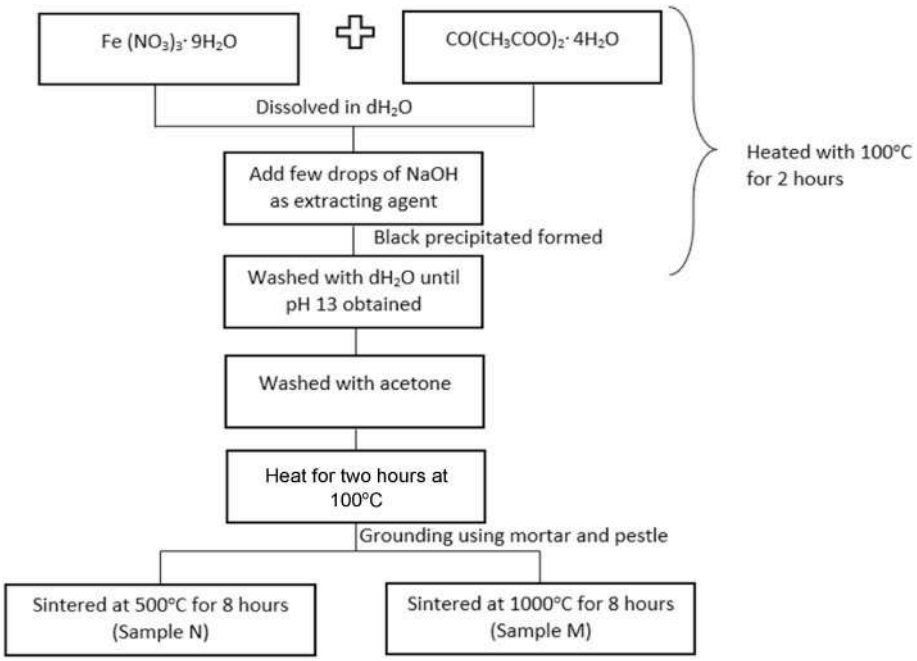

Fig. 1. Summary of synthetization of $CoFe_2O_4$ particles.

Table 1
Summary of synthesized $CoFe_2O_4$ particles and samples of MRG.

Sample's name	Description
M	Micro-sized of $CoFe_2O_4$ particles
N	Nano-sized of $CoFe_2O_4$ particles
O	MRG
M1	MRG +1 wt % of micro-sized $CoFe_2O_4$
N1	MRG +1 wt % of nano-sized $CoFe_2O_4$

$CoFe_2O_4$ particles was tabulated in Table 1.

The samples were then characterized in terms of rheological properties correspond to various parameters. Rheometer, model MCR 302 from Anton Parr, Grazz, Austria was used to test the viscous behaviour of MRG samples under rotational mode, and with induced of different currents respective to different magnetic fields. Parallel plates (PP) of the rheometer's sample stage that having a diameter of 20 mm were used and the gap between the parallel plates was kept constant at 1 mm. During the test, the shear rate was applied within the range of 0.01–100 s^{-1} under various magnetic fields and the test was carried out at room temperature of 25 °C. The shear and yield stress as part of the viscous behaviour of MRG samples would also be extracted from the viscosity data analysis.

On the other hand, heat-related characteristics of MRG incorporated with nano- (N1) and micro-sized of $CoFe_2O_4$ (M1) were investigated via differential scanning calorimetry (DSC) concerning the phase transitions that occurred in the samples, respective to the elevated temperatures. Prior to the test, a DSC-60 instrument procured from the Shimadzu Corporation (Japan) was utilized and the measurement was conducted in a nitrogen gas atmosphere, with the flow rate of 300 ml/min. MRG samples (O, M1 and N1), about of 20 mg each was placed in an aluminum pan, individually and then be subjected to the heating environment from 25 to 400 °C, with the heating rate of 10 °C/min. Phase changes observed in the samples were then be analyzed.

Nevertheless, with the aim to observe the morphological characteristics of MRG samples, especially with N and M particles, the samples were smeared on the glass slide and immersed in n-hexane solution to extract the base oil from the grease. Then, the samples were left to dry at room temperature for 24 h. A thin layer that formed on the glass slide was scoped and put onto the sample holder before being coated with gold-coater for 2 min. Then, the dried-MRG structure was analyzed by using field emission scanning electron microscopy (FESEM), model ZEISS from Merlin, Germany. Meanwhile, the cross-section width of the thickeners was measured by using ImageJ software analysis.

In addition, Raman spectra analysis for all MRG samples were conducted to investigate the chemical structure and molecular interactions of chemical bonds that changed within the sample respective to N and M particles added. The characterization was carried out by using Micro-Confocal Raman Spectrometry that equipped with Nikon eclipse C*i*-type, from Tokyo, Japan. This testing was employed with a green laser (NRS 1500W) that supplied a wavelength of 532.04 nm, which cover a Raman shift range from 100 cm^{-1} to 1800 cm^{-1}. Then, the acquired spectra was analyzed by using uSoft software to determine the changed of peaks correspond to the changed of chemical bonding in the MRG.

3. Results and discussion

3.1. Properties of $CoFe_2O_4$ particles

Fig. 2 presents the morphological characteristics of N and M that were sintered at 500 °*C* and 1000 °*C*, respectively. It is clear from the FESEM images that as the sintering temperature increased, the size of the $CoFe_2O_4$ particles has shown significant changes. As in Fig. 2(a), with 1000 °*C* of sintering temperature, the M formed in polygonal shape with facet edges in 2.5 μ m of average size. This is due to the particles selectively growing in ease orientations that facilitate the formation of polygonal structures [47]. In this case, high sintering temperature would induce more energy for the mobility of atoms thus led the growth of crystals in preferential directions of <100>, followed by < 110> and <111>, forming symmetrical branches of $CoFe_2O_4$. Then, the particles grew into spaces between branches completing the polygonal shape of $CoFe_2O_4$ in {111} crystallographic planes [48]. In contrast, for N that was sintered at 500 °C, the particles afford to form small spherical shape since the growth was suppressed after formation of solute crystal of $CoFe_2O_4$, and the ranging size is around 10–20 nm. However, it was noted that the nanoparticles tend to agglomerate and form a large clump due to the small distance of inter-particle and high surface energy [49, 50].

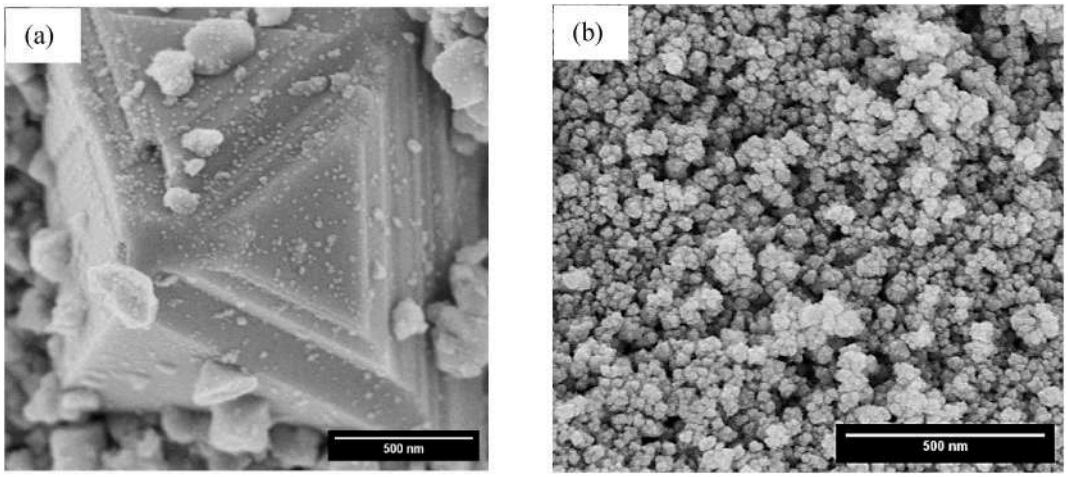

Fig. 2. FESEM images of the synthesized $CoFe_2O_4$ particles for (a) M that was sintered at 1000 °*C* and (b) N that was sintered at 500 °*C*..

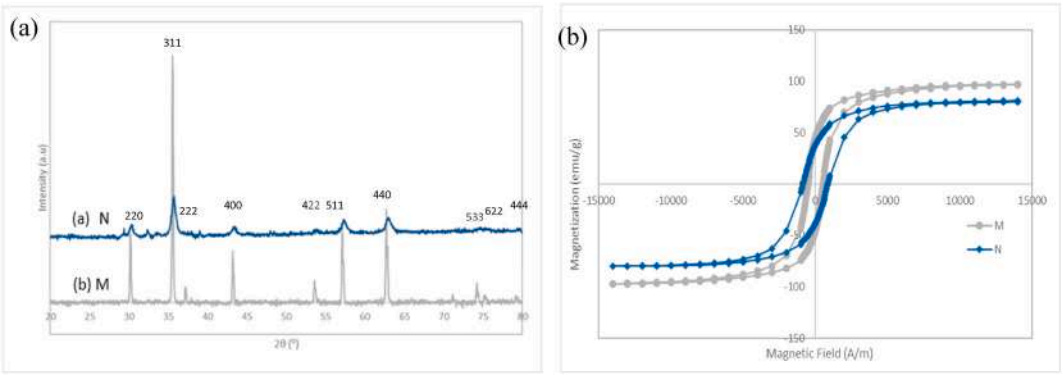

Fig. 3. (a) XRD patterns of the synthesized nano- (N) and micro-$CoFe_2O_4$ (M) which confirm the formation of the particles, and (b) Magnetic hysteresis loops of the synthesized $CoFe_2O_4$ particles that show the magnetization of M is higher as compared to N.

Fig. 3 depicts the XRD pattern and magnetic hysteresis loop for M and N of $CoFe_2O_4$ particles. As shown in Fig. 3 (a), the XRD patterns obtained from both samples are identified and agreeable with references of JCPDS card no. 98-018-4063 which indicates the formation of cubic crystal structure of $CoFe_2O_4$ with Fd-3m of space group. Based on the peaks obtained for both powders, it can be observed that no extraordinary peak was detected, showing no impurities of synthesized $CoFe_2O_4$ particles detected. It is also noted that although different sintering temperatures were applied to the particles, the XRD diffraction peaks somehow resulted similar as falls in the same Bragg's angles at 30.23°, 35.61°, 37.25°, 43.28°, 53.70°, 57.25°, 62.87°, 74.39°, 75.45°, and 79.39°, individually. In fact, for M, the peaks observed are sharper and narrower as compared to the peaks of N attributed to the larger size of particles, micro-$CoFe_2O_4$ which is subsequently influenced by its domain size [51]. Nonetheless, the diffraction pattern of both XRD analysis has shown the spinel phases of $CoFe_2O_4$ which confirms the formation of the respective particles.

Meanwhile, Fig. 3(b) demonstrates the magnetic hysteresis loops for $CoFe_2O_4$ particles, particularly for M and N. As shown in the figure, the magnetic saturation, M_s of sample M is higher as compared to N that was sintered at lower temperature, which is by 20 % difference where the M_s for M and N is about 97.14 and 80.70 emu/g, respectively. The difference in the magnetization value of synthesized particles is due to the alteration of the particles sizes that significantly changed the micromagnetic structure of the particles. It is believed for sample M that exhibited larger size of particles, there is a redistribution of cations where the Fe^{3+} ions tend to migrate more on the octahedral sites which resulted in the increment of the magnetization value of the microparticles [52]. Meanwhile for N, a lower value of the magnetization, M_s is due to the disordered surface resulting in non-collinearity of the magnetic moments exhibited by the finite size of the nanoparticles [53]. However, in terms of the coercivity (H_c) and retentivity (H_r), the sample N recorded higher value than the sample M. This indicated that the nanoparticles of $CoFe_2O_4$ (N) require more magnetic field to be demagnetized (H_c) and remain higher residual magnetism when magnetic field was removed from the particles (H_r), as contrast with the micro-particles of $CoFe_2O_4$ (M). It also shows the softer magnetic particles of M as compared to N. The summary of the magnetic properties of synthesized $CoFe_2O_4$ particles are tabulated in Table 2.

3.2. Viscosity of MRG samples with $CoFe_2O_4$ particles

In order to investigate the viscous behavior of MRG samples with different sizes of $CoFe_2O_4$ (M1 and N1), a rotational mode of rheological test was carried out with applied shear rates between 0.01 and 100 s^{-1}, and each test underwent different values of magnetic field. As a result, the viscous behavior of MRG samples in terms of viscosity, shear stress and yield stress were extracted and further analyzed. Fig. 4 depicts the

Table 2
Magnetic properties of $CoFe_2O_4$ particles.

Samples	Magnetic Saturation, M_s (emu/g)	Coercivity, H_c (A/m)	Retentivity, H_r (emu/g)
N	80.70	865.63	45.72
M	97.14	509.05	38.08

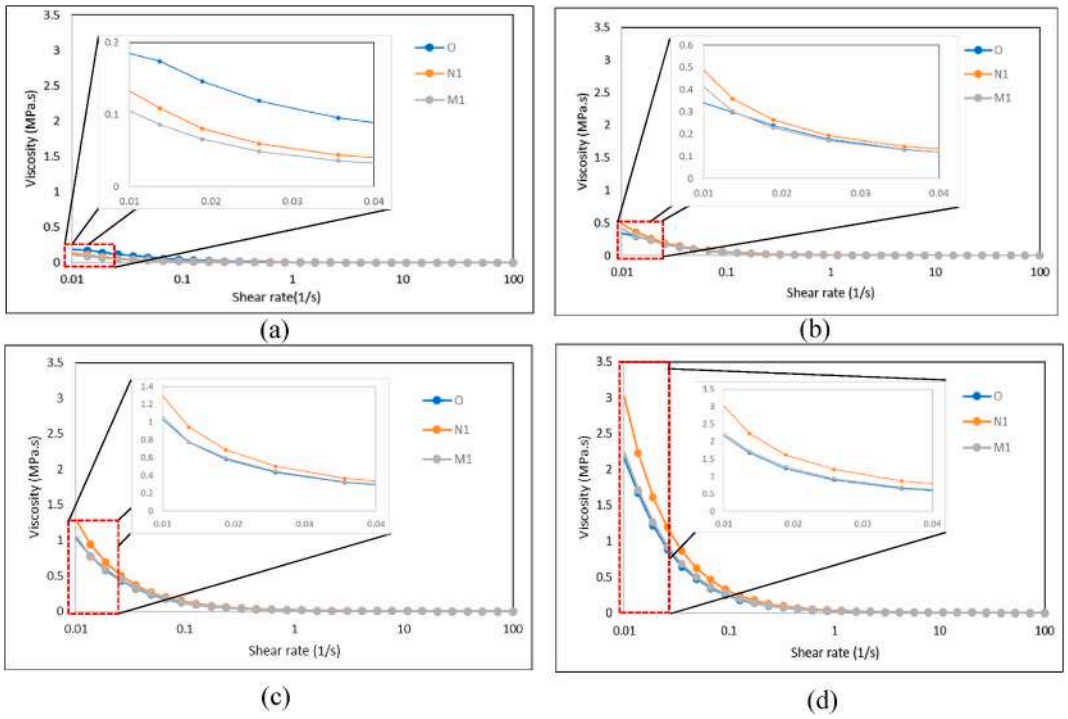

Fig. 4. Viscosity of MRG samples versus shear rates, under different applied magnetic fields for (a) 0 T (b) 0.181 T (c) 0.383 T and (d) 0.596 T.

viscosity effect of MRG samples, with magnified areas indicating a significant difference in each MRG sample correspond to O, M1 and N1. Meanwhile, Table 3 tabulated the viscosity values of all MRG samples at different magnetic fields.

Based on Fig. 4, it is clearly observed that all MRG samples exhibited shear thinning effect where, as the shear rate increased, the viscosity of the samples decreased exponentially, for both off- and on-state conditions. Particularly in the absence of magnetic field (0 T) as depicted in Fig. 4 (a), sample O demonstrated higher initial off-state viscosity, around 0.185 MPa s followed by N1 and M1 which are 0.137 and 0.105 MPa s, respectively. This indicated that the addition of $CoFe_2O_4$ either in micro- or nano-sizes have decreased the initial off-state viscosity of the MRG. In fact, M1 possess 15 % viscosity lower than N1 due to more disentanglement of the grease fibrous structure with micro-$CoFe_2O_4$ [19]. Basically, at the off-state condition, nature of the grease would depend on the fibrous structure of the thickener, and it primarily determines the viscous behavior of the material. The grease thickener would act as a 'sponge' which absorb and release the base oil [54,55]. As shown in Fig. 5 (a), the fibrous structure of MRG (O) exhibited in more degree of entanglement and eventually not affected by the incorporation of the CIP. However, with the presence of micro-$CoFe_2O_4$ (M) in the MRG, the larger size of additive with facet edges shape caused more random internal friction among the particles which might generate heat during the mixing process of M1. Therefore, the weak molecular bond of the thickener's structure including van der Waals and hydrogen bonds tend to break-up, and the base oil that is kept in the grease thickener structure would be released, as shown in Fig. 5 (b). This phenomenon led to the reduction of the viscosity of M1 [56]. Besides, larger size of M caused more disentanglement of the fibrous structure of grease and more base oil in the grease medium has been released, resulting in larger decrement of the initial off-state viscosity of the material.

Nevertheless, for N1 sample, the reduction of the initial off-state viscosity is caused by the nanoparticles size of $CoFe_2O_4$ which filled in the voids of the fibrous thickener structure of the grease that basically contained of base oil. As a result, the base oil would be discharged from the fibrous structure of grease that subsequently caused the N1 to become less viscous. In fact, the discharged base oil to the MRG might act as a plasticizer that increased the lubricity in the grease medium. However, the initial off-state viscosity of N1 is greater than the M1 although it has successfully reduced as compared to O, by 31.6 % reduction. This result can be explained due to the larger number of particles introduced in the MRG with 1 wt % of $CoFe_2O_4$ nanoparticles, as contrast with 1 wt % of micron-$CoFe_2O_4$. Thus, the density of the total particles (CIP and N) that were incorporated into the grease would be higher which subsequently increased slightly the resultant viscosity of N1. As illustrated in Fig. 5 (c), the fibrous structure of N1 has become denser with the localized of $CoFe_2O_4$ nanoparticles in the voids of thickener structure. Although, in return the base oil has been released that reduced the initial off-state viscosity of MRG, the localized nano-additive in the fibrous structure has slight increased the entanglement degree of the fibrous structure itself.

On the contrary, at the on-state condition, the N1 became more viscous followed by M1 and O, as depicted in Fig. 4(b–d) and as listed in Table 3. In particular, the initial on-state viscosity of N1 is around 0.49 MPa s at 0.181 T, about 277 % increment from the off-state condition and the value has further increased to 3.02 MPa s when the magnetic field was increased to 0.596 T. Meanwhile, for M1, the improvement of the initial on-state viscosity is still notable, specifically by 273 % for 0.41 MPa s (0.181 T) as compared to the off-state condition. However, the increment of the on-state viscosity of sample O is about 89 % only, from 0 to 0.181 T, before the viscosity value has further increased to 2.16 MPa s when the magnetic field was increased to 0.596 T. The least increment of the viscosity from off-to on-state condition is due to smaller disentanglement of grease fibrous structure as shown in Fig. 6 (a). This indicated that the additives either in micron- or nanosized $CoFe_2O_4$ has

Table 3
Viscosity values for all MRG samples at different magnetic fields.

Samples	Viscosity (MPa.s)			
	0 T	0.181 T	0.383 T	0.596 T
O	0.185	0.340	1.035	2.163
N1	0.137	0.487	1.295	3.021
M1	0.105	0.413	1.064	2.238

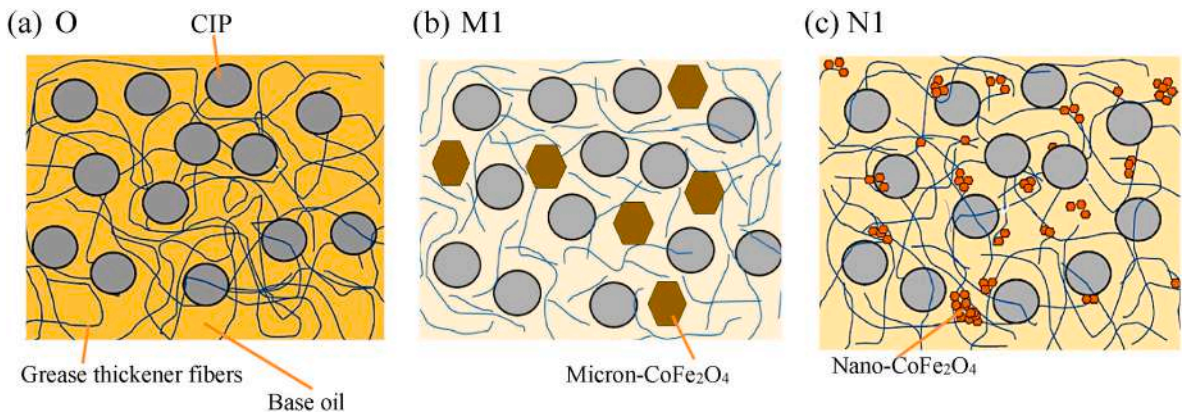

Fig. 5. Illustrations of the structure in MRG samples respective to the initial off-state viscosity for (a) MRG (O), (b) MRG with $CoFe_2O_4$ micron-particles (M1) and (c) MRG with $CoFe_2O_4$ nanoparticles (N1) (The background colors indicate the viscosity level of the samples less viscous).

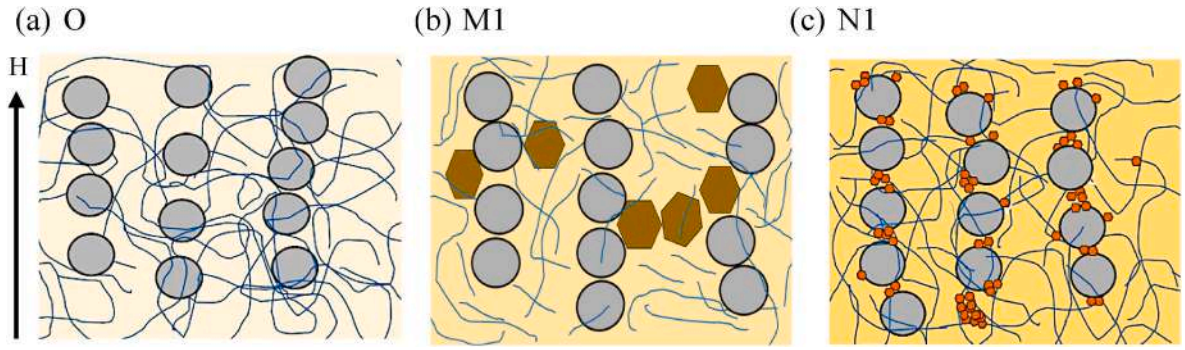

Fig. 6. Illustrations of the structure in MRG samples at the initial on-state viscosity for (a) MRG (O), (b) MRG with $CoFe_2O_4$ micro-particles (M1) and (c) MRG with $CoFe_2O_4$ nanoparticles (N1) (The color indicates the viscosity level of the MRG samples less viscous).

significant influenced on the viscosity changes of the MRG, for both conditions. The rise in the viscosity value of MRG samples from off-to on-state conditions is due greater responsiveness of the magnetic particles (CIP and $CoFe_2O_4$) towards the applied magnetic field and formation of a stronger chain-like particles proportional to the strength of magnetic fields.

In the case of M1, due to similar size of M with CIP, the additive tends to attach amongst the CIP and simultaneously improved the strength of chain-like particles as illustrated in Fig. 6 (b). The large surface area of facet shape of M has high tendency to align and fill in the spaces between the arrangement of CIP due to high magnetization exhibited by the particles. Meanwhile, for N1, the nanosized of N are prone to attach and surrounded the surface of CIP and formed cloud structure due adsorption and magnetic forces towards the CIP, and it simultaneously inhibited the CIP from being agglomerated that primarily favored by the van der Waals and magnetic attractions [57,58]. As a result of magnetic forces between those magnetic particles, it led the cloud-N to fill up the spaces between the CIP and subsequently enhanced the chain-like structure of the particles towards the magnetic fields as shown in Fig. 6 (c). These two phenomena somehow contributed to the improvement of the viscosity of MRG at the on-state condition. In fact, higher density of N has further enhanced the on-state viscosity of N1 as compared to M1.

Despite that, in terms of shear rates that were applied between 0.01 and 100 s^{-1}, it is discovered that, beyond the shear rate of 0.1 s^{-1}, particularly at any magnetic field, the MRG samples tend to exhibit the same value of viscosities for with or without the additives. The presence of additives has no impact on the viscosity of MRGs. At the moment, the sample O, M1 and N1 have entered the viscous flow region attributed to the base oil separation happened in the grease medium. Therefore, based on current findings, the safety shear rates that can be used for the MRG especially with incorporated of $CoFe_2O_4$ as additives is less than 0.1 s^{-1} in order to maintain the principle working of MRG and the significant role of additives towards the viscosity alteration at any condition.

3.3. Shear stress of MRG samples with $CoFe_2O_4$ particles

Fig. 7 depicts the relationship between shear stress and shear rates of MRG samples with micron- and nanosized of $CoFe_2O_4$ under different magnetic fields induction. In brief, the shear stress increased as the shear rates and magnetic fields increased. In Fig. 7 (a), with the absence of magnetic field, it represents that M1 possessed the lowest shear stress as compared to N1 and O, especially with the shear rates of below than 0.1 s^{-1}. In fact, with the increment of shear rates, M1 shows very slow increasing trend up to 1.2 s^{-1} and it is where the yield point of M1 was identified, as in dotted red circle. Meanwhile for N1, the slight increment in shear stress was observed until small peak was noted, around 0.5 s^{-1} and it is identified as the yield point of N1. This shows that at the off-state condition, although the applied shear rate for N1 is less than M1, the shear stress that can be sustained by N1 is greater before the transition of semi-solid behavior to flow region of MRG would be taken place. This is also correlated with the higher off-state viscosity of N1 as compared to M1, as discussed in previous section. On the other hand, sample O shows an increasing trend of shear stress gradually with shear rates and exhibited the highest value of shear stress. Similarly, it is due to highest off-state viscosity of O (0.19 MPa s) as compared to M1 (0.11 MPa s) and N1 (0.14 MPa s) that could sustain higher stress upon deformation. Basically, the yield point in MRG samples is due to the slip phenomenon that occurred between the particles and grease medium that break-up the interaction between both components upon shearing

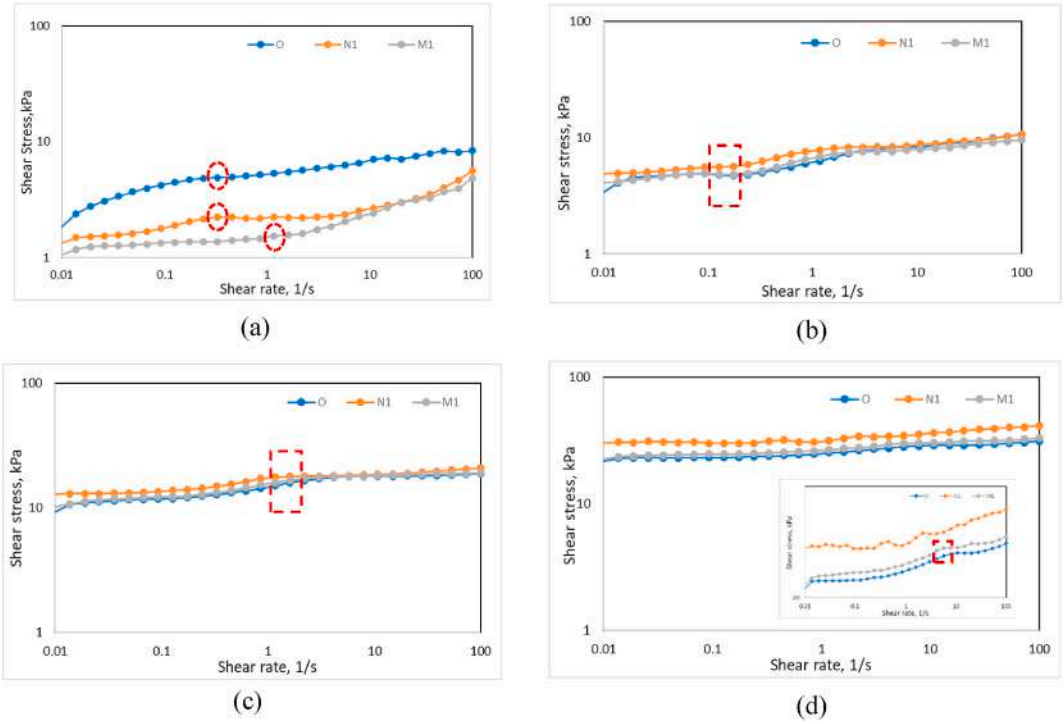

Fig. 7. Shear stress of MRG samples as a function of shear rates under different value of magnetic fields of (a) 0 T, (b) 0.181 T, (c) 0.383 T and (d) 0.596 T.

effect.

On the contrary, when magnetic fields were applied to the MRG samples, the shear stress increased as the shear rate increased as shown in Fig. 7(b–d). It is known that the increment of shear stress in MRGs is due to the formation of stronger dipole-dipole interaction among the magnetic particles, including CIP–CIP, CIP–$CoFe_2O_4$ and $CoFe_2O_4$–$CoFe_2O_4$, and towards the magnetic fields. In addition, N1 recorded the highest trend of shear stress, followed by M1 and O for all values of applied magnetic fields. Nevertheless, all MRG samples possessed the similar shear rate, about 0.2 s^{-1} for 0.181 T, 1.0 s^{-1} for 0.383 T and ~9 s^{-1} for 0.596 T that caused the yield point to occur in each MRG sample, before shear stress were escalating with higher shear rates for all conditions. For instance, at 0.181 T and with 0.2 s^{-1} shear rate, N1 achieved the highest yield stress about 4.87 kPa, followed by M1 at about 4.12 kPa and O with 3.40 kPa. Then, the shear stress was still dominant by N1 with increased shear rates. This phenomenon is most likely due to higher on-state viscosity that exhibited by N1, with the aid of the nano-$CoFe_2O_4$ in the MRG which increased the density, the magnetic interactions of magnetic particles towards the magnetic field as well as the flow resistance during the shearing effect. Similar phenomenon occurred in sample M1 and O. On the other hand, as observed in Fig. 7 (d) with magnified area, although N1 recorded the highest shear stress, the graph has shown fluctuated might be due to more slippage occurred between the particles, attributed to the larger number of particles in the MRG which experienced shearing and magnetic strength effects. Nevertheless, based on the findings, both micron- (M) and nano-$CoFe_2O_4$ (N) have enhanced the shear stress of MRG at the on-state conditions, somewhat similar to sample O and even higher although both additives have reduced the respective off-state viscosity of the MRG.

3.4. Yield stress of MRG samples with $CoFe_2O_4$ particles

In most MR devices, particularly in MR brake and MR damper, the yield stress is one of the salient parameters to evaluate the efficiency of the device. In fact, it is noted that high value of yield stress would result in high braking torque thus, enhancing the efficiency of MR devices. In brief, yield stress is the minimum shear stress required to rupture the formation of chain-like alignment of magnetic particles in the MRG that formed due to interactions of magnetic particles towards the magnetic field and shearing force. The yield stress of all MRG samples in both off- and on-state conditions were projected from Fig. 7 and presented in Fig. 8 below. As can be observed in Fig. 8, at the off-state condition (0 T), sample O performs higher yield stress of around 1.84 kPa as compared to N1 (1.33 kPa) and M1 (0.17 kPa) due to higher flow resistance by high entanglement density of the grease thickener's structure. This is also corresponded to its highest off-state viscosity of the MRG compared to other two samples.

Meanwhile, at the on-state conditions from 0.181 to 0.596 T, N1 possessed the largest enhanced yield stress and its trend preceded for other values of magnetic field. The trend followed by M1 and O which both exhibited almost similar yield stress for all applied magnetic fields. This indicated that with higher magnetic field strength, the interaction of magnetic particles in the MRG increased which caused stronger chain-like alignment of the particles towards the magnetic fields. Thus, the MRGs become more viscous and exhibited higher flow resistance upon

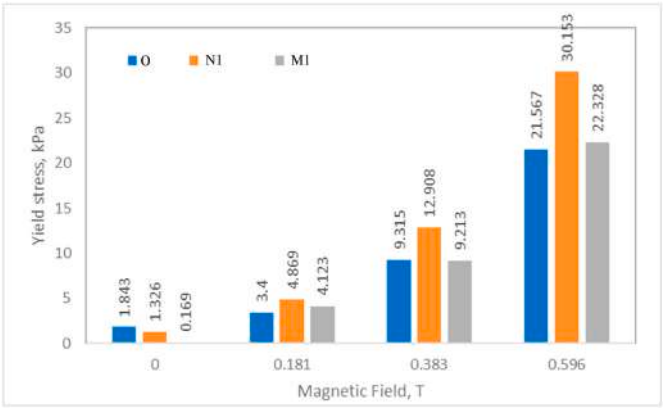

Fig. 8. Yield stress of all MRG samples at different values of magnetic field.

shearing force. In return, it requires greater yield stress to cause slip phenomenon between the particles and grease medium that result in transition from solid-like medium to flow region. Besides, as presented in the figure, N1 have higher yield stress attributed to greater on-state viscosity than M1 and O, as have been discussed in previous section. The finding somehow shows that although the addition of M and N have reduced the off-state viscosity of MRG, the improved responsiveness of M1 and N1 towards the applied magnetic fields has been enhanced that leastwise maintain the shear and yield stress of the MRG without additives. Therefore, the addition of M and N have covered both improvement targets; in reducing the off-state viscosity and improving the on-state shear and yield stress of MRG. As compared with previous study that tabulated in Table 4, this study has been enhance the value of MRGs' yield stress with addition of $CoFe_2O_4$.

3.5. DSC analysis of MRG samples

DSC measurements were conducted to investigate the phase transitions of MRG samples correspond to different temperatures, from 25 °C (ambient temperature) to 400 °C. Based on Fig. 9, heat flow (mW/mg) was observed to be more negative indicating the heat absorbed by the samples as temperature increased, and patent of peaks were noted similar for all the samples. The distinct peaks were marked as P_1, P_2 and P_3, respectively. The first peak (P_1) which correspond to endothermic reaction would represent the melting point of the lithium grease thickener. It was found that the melting point of lithium grease thickener for O, M1 and N1 were similar, around 200 °C designating that the heat induced has softened the grease causing it began to flow. Meanwhile, the incorporation of micron- (M) and nano-$CoFe_2O_4$ (N) in the MRG has no significant effect on the melting point of lithium grease thickener, which is at 200 °C as similarly stated by Moreno et al. [59]. As compared with MRG-N1, peaks of MRG with micro-sized of $CoFe_2O_4$ are sharper and more dipped due to the faster rate of transformation where it absorbs more heat energy to melt the grease thickener by 3.95 mW/g of heat. As the temperature increased to 353.11 °C, the second peak which belongs to exothermic reaction (P_2) appeared for N1 only. As heat released by the grease structure around this temperature, the localized of $CoFe_2O_4$ nanoparticles in the voids of thickener structure as discussed in previous section caused it to be aggregated, simultaneously with the degraded MRG. Remarkably, with the increment of temperatures in the range 367–400 °C, all the three samples showed exothermic reactions (P_3) which manifests the possibility of more aggregation of the particles occurred, including the CIPs and $CoFe_2O_4$ in the grease medium [60]. Based on the finding, practical operation of the MRG upon incorporation of the $CoFe_2O_4$ as additive should not be above than 200 °C considering the thickening behavior of the lithium grease based MRG.

Table 4
Comparison data with the previous research regarding on the off-state viscosity and on-state yield stress.

Additives		Viscosity (Pa.s)	Yield Stress (Pa)	Ref
Type	Size			
Chromium Oxide	~100 nm crossectional length	–	500 (0.1T)	[24]
Meghamite	10 nm	~50000	–	[28]
Graphite	3 μm	49000	11000 (0.181T)	[26]
Molybdenum disulphide	2 μm length	1600	6000 (0.36T)	[25]
Cobalt ferrite	1–3 μm	137000	4869000 (0.181T)	This study
	10 nm	105000	4123000 (0.181T)	

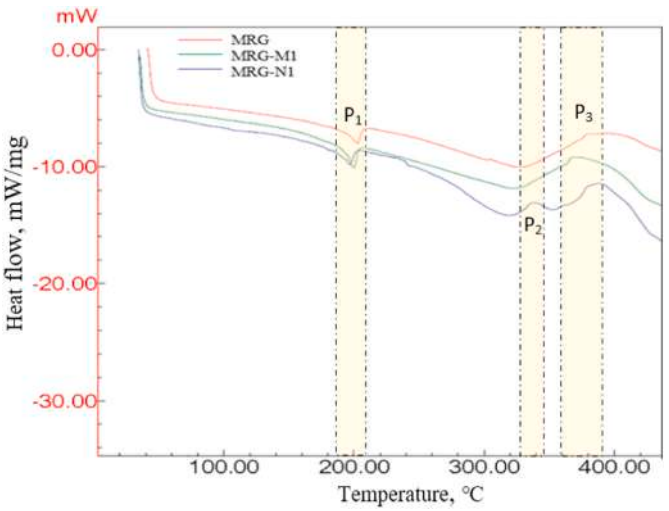

Fig. 9. DSC curves for all MRG's samples correspond to temperature range of 25–400 °C.

3.6. Morphology analysis of MRG samples with $CoFe_2O_4$ particles

Fig. 10 depicted the morphological characteristics of dried grease, and dried MRGs particularly O, M1 and N1 in which the base oil was removed from the grease structure. The micrographs were observed via FESEM. As shown in Fig. 10 (a), the thickener structure of the pure grease can be clearly seen where the structure portrayed in the form of entangled fibrous with the average width around 50 nm. Meanwhile, Fig. 10 (b) presents the micrograph of MRG sample (O) which shows that the fibrous structure of the grease thickener has been enclosed the spherical CIPs and the average fibrous width was noted around 80–100 nm.

However, a difference between the thickener structure of M1 and N1 have been observed as in Fig. 10 (c) and (d), respectively in terms of the fibrous structure and cross-sectional width of the grease thickener itself. For M1, the observed thickener's length became shortened and less entangled as compared to N1 and as measured for M1, the width of the thickener structure is around 150–200 nm. In fact, as noted in Fig. 10 (c), the M which is in facet-shape particles caused it to be faced-positioned among the spherical CIPs and its sharp edges has simultaneously break-up the bonds of the thickener structure of the grease. Thus, the 'twisting' fibrous structure of grease seems untie or detangled that caused increment in its average width value. On the other hand, as discovered in Fig. 10 (d), the N has been attached on the surface of CIPs and most likely would be "trapped" or fill in the voids of the thickener structure of the grease. As a result, the fibrous structure of grease has been liberated that led to increase in the value of the fibrous width slightly, to ~114 nm as compared to sample O. Both phenomena in M1 and N1 also caused the releasement of base oil from the fibrous grease structure as has been discussed in Fig. 5. This finding also in line with the decrement of the initial off-state viscosity of the MRG sample and conclusively the viscosity of MRG is highly dependent on the thickener's structure of the grease.

3.7. Raman spectra analysis of MRG samples

Fig. 11 shows the Raman spectra for sample O, M1 and N1, respective to without and with the $CoFe_2O_4$ particles in the MRG. In brief, Raman spectrum for all the samples exhibited the same pattern of peaks, which originated from the molecular interactions of the grease and the particles. The first Raman peak at the range below 500 cm^{-1} was observed to be similar for sample O, M1 and N1, and it has been identified as metallic oxides bond which correspond to the CIP and $CoFe_2O_4$ (M and N) particles in the MRG samples. In fact, the intensity of M1 and N1 are

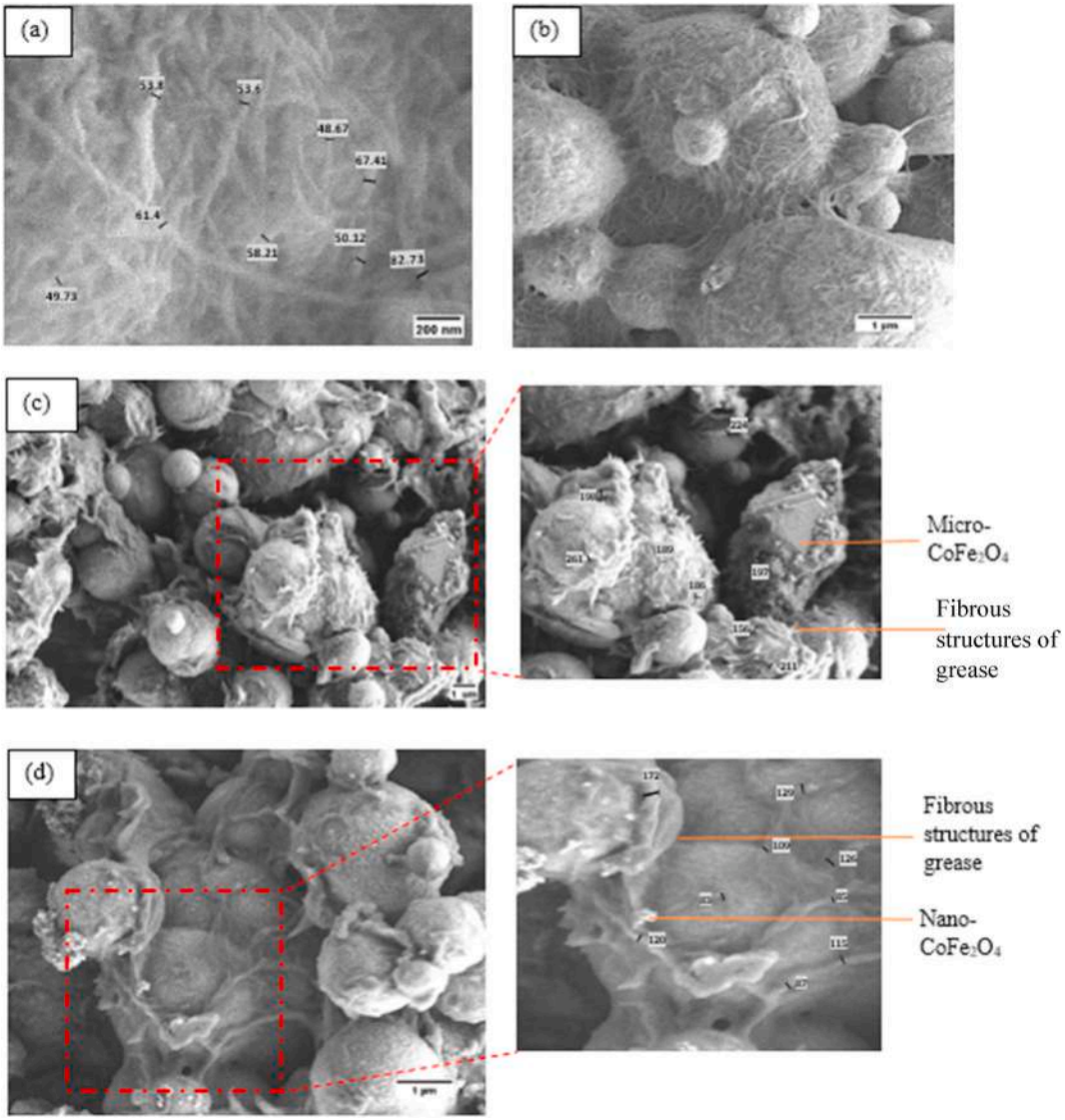

Fig. 10. FESEM micrographs of MRG samples for; (a) pure grease; (b) O; (c) M1 with magnified area and (d) N1 with magnified area.

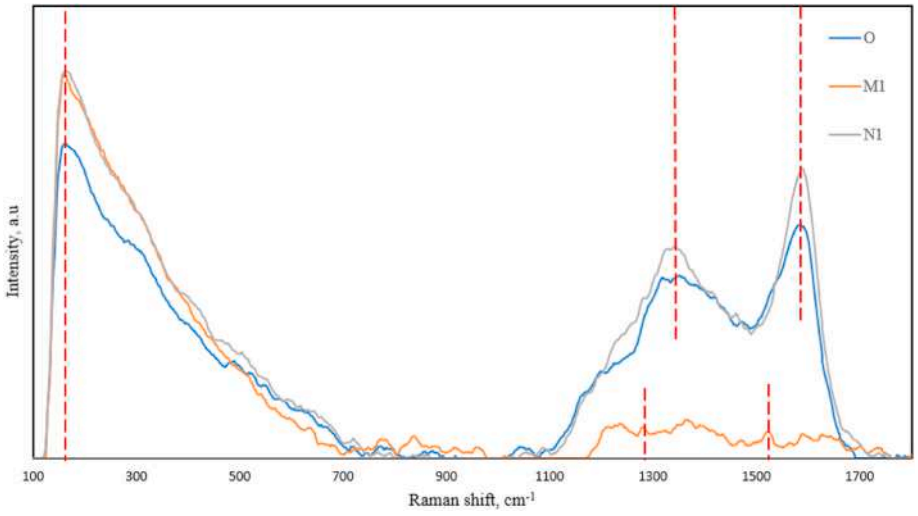

Fig. 11. Raman spectra of MRG samples between the range 100–1800 cm^{-1} of Raman shift.

recorded higher as compared to sample O indicating the amount of metallic bonds (iron, cobalt and iron oxides) have been increased, attributed to the amount of CIP and $CoFe_2O_4$ particles presented in the grease medium. Meanwhile, in the range of 1300–1700 cm^{-1} of Raman shift, the second and third peaks were observed belong to methyl (C–H) bond and covalent double bond (C=O), respectively which both bonds are owned by the thickener structure of the grease [61]. In fact, sample O and N1 show the similar Raman shift for C–H bond, at 1348 cm^{-1} and C=O bonds at 1578 cm^{-1}, unlike for sample M1 that has the Raman peak for C–H and C=O bonds shifted more to the left, around 1356.5 and 1584.3 cm^{-1}, respectively as illustrated in the figure. These observations might be due to the fibrous structure of the grease that has been changed in response to either micro- or nano-$CoFe_2O_4$ added to the MRG. In fact, the addition of micro-$CoFe_2O_4$ (M) in the MRG has caused disentanglement of the fibrous structure of the grease which simultaneously disrupted or reduced the levels of C–H and C=O bonds in the fibrous structure of the grease. The base oil in the grease thickener structure also has been released as which leads to the reduction of the initial off-state viscosity of MRG, as discussed in the previous section. This structural modification also might lead to the shifted of the Raman peak of C–H and C=O bonds for M1, as compared to N1 and O. Meanwhile, for N1, the presence of nano-$CoFe_2O_4$ has localized the nanoparticles inside the fibrous structure of the grease and this phenomenon might pronounce the C–H and C=O bonds become more compact and suggesting a stronger thickener structure of the grease. Correspondingly, the Raman peaks for C–H and C=O bonds for the N1 is higher as compared to sample O (MRG). Thus, the presence of two distinct sizes of additive has shown a significant affect towards the alteration of the molecular structures and bonding in the MRG.

4. Conclusion

In this study, different sizes of $CoFe_2O_4$ in terms of micron- (M) and nanoparticles (N) have been utilized to investigate the role of additives on the viscous behavior of the MRGs. Three samples were prepared which were MRG without the $CoFe_2O_4$ (O), MRG-micron $CoFe_2O_4$ (M1) and MRG-nano $CoFe_2O_4$ (N1). Prior to the fabrication of MRG samples, the additives have been synthesized via co-precipitation method with different sintering temperatures of 500 °C for M and 1000 °C for N. It shows that M has formed in polygonal shape with 2.5 μ m in average size while N is in spherical shape with 10–20 nm in average size. M also recorded higher magnetization value, M_s by about 20.37 % more than M_s of N attributed to the larger size of particles. Meanwhile, based on the DSC analysis, there is no significant changes on the melting point of MRG, around 200 °C although 1 wt % of micro- (M) or nano-$CoFe_2O_4$ (N) particles were added in the MRG. As the additives were incorporated into the MRG with 1 wt % concentration, separately, both M1 and N1 have successfully reduced the initial off-state viscosity of the MRG, by 43.2 % for M1 and 26 % for N1 as compared to O. M1 decreased the off-state viscosity of MRG by disentanglement of the fibrous structure of the grease by M while N has prone to fill-in the gap between the fibrous thickener's structure of the grease. Simultaneously both phenomena caused discharging of the base oil of the grease and reduced off-state viscosity of the MRG while role of M during disentanglement of the fibrous structure has resulted more reduction of the off-state viscosity value as compared to N. It discovered that with $CoFe_2O_4$ particles, the width of fibrous structure of the grease became larger as compared to fibrous structure of MRG without the additives. Nevertheless, N1 possessed higher on-state viscosity, followed by M1 and O due to enhanced chain-like particles in the MRG towards the magnetic fields. Thus, MRG with the additive become more viscous and solid-like state, and it correlates with the enhanced of shear and yield stress of the MRGs at the on-state conditions. Indeed, the yield stress of N1 and M1 has been improved by 39.8 % and 3.5 %, respectively as compared to MRG (O). On the hand, respective to the chemical analysis by Raman spectroscopy, the C–H and C=O bonds which are designated for the fibrous thickener structure of the grease has been shifted to the left when M was added to the MRG (M1). It is accompanied with the decrement in intensity of the bonds due to disentanglement of the fibrous structure of the grease which resulted in the collapsing of the bonds. Meanwhile, the Raman shift for the C–H and C=O bonds, particularly for N1 and O are noted similar, indicating the structure bonds have been maintained although N was added into the MRG. Therefore, it can be concluded that different sizes of additives would play different roles in modifying the viscous behavior of MRG which could provide significant knowledge and information for researchers to utilize suitable sizes of additive for specific requirements. Meanwhile, for the future works, further investigation related to transient response of MRG, incorporated with these additives will become essential to evaluate the time taken for modified MRG composite to response towards the applied stimulus.

Data availability

Data will be made available on request.

Declaration of competing interest

The authors declare the following financial interests/personal relationships which may be considered as potential competing interests: Nur Azmah binti Nordin reports financial support was provided by Universiti Teknologi Malaysia Malaysia-Japan International Institute of Technology. Ubaidillah reports financial support was provided by Sebelas Maret University. If there are other authors, they declare that they have no known competing financial interests or personal relationships that could have appeared to influence the work reported in this paper.

Acknowledgment

This study has been funded by Universiti Teknologi Malaysia (UTM) Zamalah (Vot No. 0060 N) and Ministry of Higher Education of Malaysia under Fundamental Research Grant Scheme (FRGS/1/2022/TK10/UTM/02/75). Also, this study appreciates partial funding from Ministry of Education, Culture, Research and Technology, Republic of Indonesia through Hibah Kolaborasi Internasional 2024.

References

[1] Mohamad N, Ubaidillah, Mazlan SA, Imaduddin F, Choi SB, Yazid IIM. A comparative work on the magnetic field-dependent properties of plate-like and spherical iron particle-based magnetorheological grease. PLoS ONE; 2018.
[2] Wang H, Chang T, Li Y, Li S, Zhang G, Wang J. Field–frequency-dependent nonlinear rheological behavior of magnetorheological grease under large amplitude oscillatory shear. Frontiers in Materials 2021;8.
[3] Bahiuddin I, Wahab NAA, Shapiai MI, Mazlan SA, Mohamad N, Imaduddin F, et al. Prediction of field-dependent rheological properties of magnetorheological grease using extreme learning machine method. J Intell Mater Syst Struct 2019;30(11).
[4] Wang H, Zhang G, Wang J. Quasi-static rheological properties of lithium-based magnetorheological grease under large deformation. Materials 2019;12(15):2431.
[5] Ye X, Mao R, Wang J. Analysis of magnetorheological grease normal force characteristics in static and dynamic shear modes. Mater Res Express 2021;8(1).
[6] Yan H, Li P, Duan C, Dong X. Studies with rheological behavior of composite lithium-based magnetorheological grease. Metals 2021;11(11).
[7] Wang K, Dong X, Li J, Shi K. Yield dimensionless magnetic effect and shear thinning for magnetorheological grease. Results Phys 2020;18(May):103328.
[8] Mohamad N, Ubaidillah, Mazlan SA, Choi SB, Aziz SAA, Sugimoto M. The effect of particle shapes on the field-dependent rheological properties of magnetorheological greases. Int J Mol Sci 2019;20(7).
[9] Ye X, Wang W, Wang J. The influence of temperature on the rheological properties of composite lithium-based magnetorheological grease. J Intell Mater Syst Struct 2022;33(18):2336–45.
[10] Sahin H, Gordaninejad F, Wang X, Fuchs A. Rheological behavior of magneto-rheological grease (MRG). Active and Passive Smart Structures and Integrated Systems 2007;2007.
[11] Ye X, Wang J. Creep and recovery behaviors of lithium-based magnetorheological grease. Frontiers in Materials 2021;8.
[12] Sukhwani VK, Hirani H. A comparative study of magnetorheological-fluid-brake and magnetorheological-grease-brake. Tribol Online 2008;3(1).

[13] Abdul Kadir KA, Nazmi N, Mohamad N, Shabdin MK, Adiputra D, Mazlan SA, et al. Effect of magnetorheological grease's viscosity to the torque performance in magnetorheological brake. Materials 2022;15(16):5717.
[14] Dai J, Chang H, Zhao R, Huang J, Li K, Xie S. Investigation of the relationship among the microstructure, rheological properties of MR grease and the speed reduction performance of a rotary micro-brake. Mech Syst Signal Process 2019; 116:741–50.
[15] Yadmellat P, Kermani MR. Adaptive modeling of a magnetorheological clutch. IEEE/ASME Transactions on Mechatronics; 2014.
[16] Kavlicoglu BM, Gordaninejad F, Wang X. Study of a magnetorheological grease clutch. Smart Materials and Structures; 2013.
[17] Strecker Z, Roupec J, Mazurek I, Machacek O, Kubik M, Klapka M. Design of magnetorheological damper with short time response. J Intell Mater Syst Struct 2015;26(14):1951–8.
[18] Khuntia S, Yadav R, Singh RC, Rastogi V. Design, development and analysis of a magnetorheological damper. IOP Conf Ser Mater Sci Eng 2020;804:012009.
[19] Tarmizi SMA, Nordin NA, Mazlan SA, Mohamad N, Rahman HA, Aziz SAA, et al. Incorporation of cobalt ferrite on the field dependent performances of magnetorheological grease. J Mater Res Technol 2020;9(6).
[20] Mohamad N, Yasser A, Fatah A, Mazlan SA, Nordin NA, Nabil M. Dilution dependent of different types of redispersing oils on. Magnetorheological Greases 2017;5(x):5–8.
[21] Kim JE, Ko J Do, Liu YD, Kim IG, Choi HJ. Effect of medium oil on magnetorheology of soft carbonyl iron particles. IEEE Transactions on Magnetics; 2012.
[22] Wang K, Dong X, Li J, Shi K, Li K. Effects of silicone oil viscosity and carbonyl iron particleweight fraction and size on yield stress for magnetorheological grease based on a new preparation technique. Materials 2019;12(11):7–9.
[23] Salomonsson L, Stang G, Zhmud B. Oil/thickener interactions and rheology of lubricating greases. Tribol Trans 2007;50(3):302–9.
[24] Park JH, Kwon MH, Park OO. Rheological properties and stability of magnetorheological fluids using viscoelastic medium and nanoadditives. Korean Journal of Chemical Engineering; 2001.
[25] Raj A, Sarkar C, Pathak M. Magnetorheological characterization of PTFE-based grease with MoS2Additive at different temperatures. IEEE Trans Magn 2021;57(7).
[26] Mohd Nasir NA, Nazmi N, Mohamad N, Ubaidillah U, Nordin NA, Mazlan SA, et al. Rheological performance of magnetorheological grease with embedded graphite additives. Materials 2021;14(17).
[27] Tarmizi SMA, Nordin NA, Mazlan SA, Ubaidillah U, Aziz SAA, Mohamad N, et al. Improvement of rheological and transient response of magnetorheological grease with amalgamation of cobalt ferrite. J Mater Res Technol 2022;23:1285–95.
[28] Mohamad N, Ubaidillah, Mazlan SA, Choi SB, Halim NA. Improvement of magnetorheological greases with superparamagnetic nanoparticles. MATEC web of conferences, vol. 159. EDP Sciences; 2018.
[29] Shokrollahi H. A review of the magnetic properties, synthesis methods and applications of maghemite. J Magn Magn Mater 2017;426:74–81.
[30] Shabatina TI, Vernaya OI, Shabatin VP, Melnikov MY. Magnetic nanoparticles for biomedical purposes: modern trends and prospects. Magnetochemistry 2020;6(3): 1–18.
[31] Rwei SP, Wang LY, Yang PW. Synthesis and magnetorheology study of iron oxide and iron cobalt oxide suspensions. J Nanomater 2013;::612894.
[32] Molazemi M, Shokrollahi H, Hashemi B. The investigation of the compression and tension behavior of the cobalt ferrite magnetorheological fluids synthesized by Co-precipitation. J Magn Magn Mater 2013;346:107–12.
[33] Nugroho KC, Ubaidillah U, Arilasita R, Margono M, Priyambodo BH, Purnama B, et al. The effect of Sr-CoFe2O4 nanoparticles with different particles sized as additives in CIP-based magnetorheological fluid. Materials 2021;14(13).
[34] Gopinath B, Sathishkumar GK, Karthik P, Charles MM, Ashok KG, Ibrahim M, et al. A systematic study of the impact of additives on structural and mechanical properties of Magnetorheological fluids. Mater Today Proc 2020;37.
[35] Aruna MN, Rahman MR, Joladarashi S, Kumar H, Devadas Bhat P. Influence of different fumed silica as thixotropic additive on carbonyl particles magnetorheological fluids for sedimentation effects. J Magn Magn Mater 2021; 529.
[36] Fernandes de Medeiros IA, Lopes-Moriyama AL, de Souza CP. Effect of synthesis parameters on the size of cobalt ferrite crystallite. Ceram Int 2017;43(5):3962–9.
[37] Jauhar S, Kaur J, Goyal A, Singhal S. Tuning the properties of cobalt ferrite: a road towards diverse applications. RSC Advances; 2016.
[38] Kaur H, Singh A, Kumar V, Ahlawat DS. Structural, thermal and magnetic investigations of cobalt ferrite doped with Zn2+ and Cd2+ synthesized by auto combustion method. J Magn Magn Mater 2019;474:505–11.
[39] Jiang X, Fan D, Yao X, Dong Z, Li X, Ma S, et al. Highly efficient flower-like ZnIn2S4/CoFe2O4 photocatalyst with p-n type heterojunction for enhanced hydrogen evolution under visible light irradiation. J Colloid Interface Sci 2023; 641:26–35.
[40] Nikumbh AK, Pawar RA, Nighot Dv, Gugale GS, Sangale MD, Khanvilkar MB, et al. Structural, electrical, magnetic and dielectric properties of rare-earth substituted cobalt ferrites nanoparticles synthesized by the Co-precipitation method. J Magn Magn Mater 2014;355:201–9.
[41] Sulaiman NH, Ghazali MJ, Yunas J, Rajabi A, By Majlis, Razali M. Synthesis and characterization of CaFe 2 O 4 nanoparticles via Co-precipitation and auto-combustion methods. Ceram Int 2018;44(1):46–50.
[42] Vinosha PA, Immaculate G, Mary N, Mahalakshmi K, Mely LA, Das SJ. Study on cobalt ferrite nanoparticles synthesized by Co-precipitation technique for photo-fenton application 26. *Mechanics*. Materials Science & Engineering MMSE Journal Open Access WwwMmseXyz; 2017.
[43] Lwin N, Othman R, Noor AFM, Sreekantan S, Yong TC, Singh R, et al. Influence of PH on the physical and electromagnetic properties of Mg-Mn ferrite synthesized by a solution combustion method. Mater Char 2015;110(3):109–15.
[44] Annie Vinosha P, Jerome Das S. Investigation on the role of pH for the structural, optical and magnetic properties of cobalt ferrite nanoparticles and its effect on the photo-fenton activity. Mater Today Proc 2018;5(2):8662–71.
[45] Dabagh S, Ati AA, Rosnan RM, Zare S, Othaman Z. Effect of Cu-Al substitution on the structural and magnetic properties of Co ferrites. Mater Sci Semicond Process 2015;33:1–8.
[46] Mohamad N, Ubaidillah, Mazlan SA, Choi SB, Aziz SAA, Sugimoto M. The effect of particle shapes on the field-dependent rheological properties of magnetorheological greases. Int J Mol Sci 2019;20(7).
[47] Peng Y, Xia C, Cui M, Yao Z, Yi X. Effect of reaction condition on microstructure and properties of (NiCuZn)Fe2O4 nanoparticles synthesized via Co-precipitation with ultrasonic irradiation. Ultrason Sonochem 2021;71.
[48] Li C, Liu X, Wu Y. Refinement and modification performance of Al-P master alloy on primary Mg2Si in Al-Mg-Si alloys. J Alloys Compd 2008;465(1–2):145–50.
[49] Kazemi M, Ghobadi M, Mirzaie A. Cobalt ferrite nanoparticles (CoFe2O4 MNPs) as catalyst and support: magnetically recoverable nanocatalysts in organic synthesis. Nanotechnol Rev 2018;7(1):43–68.
[50] Sangsuriyonk K, Paradee N, Rotjanasuworapong K, Sirivat A. Synthesis and characterization of CoxFe1−xFe2O4 nanoparticles by anionic, cationic, and non-ionic surfactant templates via Co-precipitation. Sci Rep 2022;12(1).
[51] Holder CF, Schaak RE. Tutorial on powder X-ray diffraction for characterizing nanoscale materials. ACS Nano 2019;13(7):7359–65.
[52] Purnama B, Wijayanta AT, Suharyana. Effect of calcination temperature on structural and magnetic properties in cobalt ferrite nano particles. J King Saud Univ Sci 2019;31(4):956–60.
[53] Ahmad SI. Nano cobalt ferrites: doping, structural, low-temperature, and room temperature magnetic and dielectric properties – a comprehensive review. J Magn Magn Mater 2022;562:169840.
[54] Salomonsson L, Stang G, Zhmud B. Oil/thickener interactions and rheology of lubricating greases. Tribol Trans 2007;50(3):302–9.
[55] Lin B, Rustamov I, Zhang L, Luo J, Wan X. Graphene-reinforced lithium grease for antifriction and antiwear. ACS Appl Nano Mater 2020;3(10):10508–21.
[56] Lugt PM. A review on grease lubrication in rolling bearings. Tribol Trans 2009;52 (4):470–80.
[57] Di N, Zhang Z, Li D, Li Z, He X. Synthesis and thixotropic characterization of micron-nanometer magnetic grease with high suspension stability. J Magn Magn Mater 2022.
[58] Dong YZ, Piao SH, Zhang K, Choi HJ. Effect of CoFe2O4 nanoparticles on a carbonyl iron based magnetorheological suspension. Colloids Surf A Physicochem Eng Asp 2018;537:102–8.
[59] Moreno G, Valencia C, de Paz MV, Franco JM, Gallegos C. Rheology and microstructure of lithium lubricating greases modified with a reactive diisocyanate-terminated polymer: influence of polymer addition protocol. Chem Eng Process: Process Intensif 2008;47(4):528–38.
[60] Maheswaran R, Sunil J. Effect of nano sized garnet particles dispersion on the viscous behavior of extreme pressure lubricant oil. J Mol Liq 2016;223:643–51.
[61] Kumar N, Saini V, Bijwe J. Tribological investigations of nano and micro-sized graphite particles as an additive in lithium-based grease. Tribol Lett 2020;68(4).